Rapid Cooperative Assembly of a Multimeric Membrane Protein Complex - Supplementary Material

James R. Thompson, Bríd Cronin, Hagan Bayley
and Mark I. Wallace*

Department of Chemistry, University of Oxford
12 Mansfield Road, Oxford, OX1 3TA, U.K.

*To whom correspondence should be addressed; E-mail: mark.wallace@chem.ox.ac.uk

Contents

1 Materials

Unless otherwise stated, all chemicals were from Sigma (Sigma-Aldrich Ltd., U.K.). Triton X–100 detergent was from Bio-Rad (Bio-Rad Laboratories, Hercules, CA). *E. coli* bacteria stocks were from Promega (Promega, Madison, WI). Rosetta cells and Protease Inhibitor Cocktail I were from Novagen (EMDBiosciences, U.K.). Doubly-deionised 18 MΩ cm water (Millipore Corporation, Billerica, MA) was used throughout unless otherwise stated. Dioxane-free isopropyl–β–D–thiogalactopyranoside (IPTG) was from Calbiochem (EMD Biosciences Inc., San Diego, CA). SDS-PAGE consumables were from Invitrogen (Invitrogen Corp. Carlsbad, CA). All chromatography consumables and Cy3B-maleimide dye was from GE Healthcare (GE Healthcare Life Sciences, Amersham, U.K.). Restriction enzymes, their buffers and additives and Phusion DNA polymerase (Finnzymes) for PCR were from New England Biolabs (New England Biolabs, Ipswich, MA).

2 Protein Labeling

The lack of any cysteine residues in wild-type α-hemolysin places no constraints on the positions at which a cysteine can be genetically engineered for subsequent chemical modification. C-terminal mutations to cysteine have been shown to affect the hemolytic activity of α-hemolysin to a lesser extent than modifications at the N-terminus [1]. Hence a construct containing a C-terminal mutant cysteine with a hexahistidine-tag for affinity chromatography was used for these experiments. α-Hemolysin T292C-NRGSGSSSGGSSH$_6$ encoded in the pT7-SC1 vector [2] was used as previously described [1, 3, 4, 5]. All DNA samples were sequenced prior to bacterial transformation.

2.1 Protein Expression and Purification

The single-cysteine mutant of α-hemolysin was prepared by overexpression in transformed BL21 Rosetta *E. coli*: F-, ompT, *hsd*S_B (r_B-, m_B-), *dcm*, *gal*, λ(DE3), pLysSRARE, Cam^r, by induction with 0.5 mM IPTG during log-phase growth. After induction, cultures were continued for a further 3 hr. Following resuspension of the cell pellet in buffer (0.1% (v:v) Triton X-100, 50 mM TRIS-HCl, 150 mM NaCl, 1 unit Protease Inhibitor Cocktail I (Novagen), 1 unit DNase 1 at pH 8.0), cells were lysed by sonication on ice, and centrifuged to pellet the debris. The cytosolic constituents were purified by immobilised metal-affinity chromatography (IMAC) using a Ni^{2+}:NTA column with a linear imidazole gradient generated by an Äkta Purifier FPLC system (GE Heathcare). The principal eluting peak was selected for labeling after its identity verification by its hemolytic activity.

2.2 Maleimide Labeling

2.2.1 Cysteine Reduction and Size-Exclusion Chromatography

Following IMAC, the protein is present in TRIS-HCl buffer with approximately 0.5 M imidazole and 0.5 M NaCl as judged by the position of the peak in buffer gradient. The pure protein sample from IMAC was incubated on ice with 1 mM DTT for 1 hr prior to gel filtration. Gel filtration was performed in degassed 20 mM TRIS-HCl buffer containing 1 mM EDTA at pH 8.0 at a flow rate of 0.5 mL min^{-1} on a Tricorn Superdex 200 10/300 GL column, in 0.5 mL batches. Successful desalting was verified by online monitoring of solution conductivity. Batches were immediately labeled with Cy3B-maleimide following elution from the column.

2.2.2 Dye-Labeling and Separation by Cation Exchange Chromatography

Labeling was carried out by the addition of a 10$\times$ molar excess of Cy3B-maleimide dye dissolved in DMF (final DMF concentration was less than 1% (v:v), dye concentration

was typically approximately 10 μM), followed by mixing in darkness and reaction at room temperature for 15 min. Folllowing this dye incubation period, a 50-fold excess (v:v) of low pH buffer was added (10 mM MES at pH 5.5, 50 mL in a typical preparation). This same low pH buffer was used to equilibrate a cation exchange column (HiTrap SPFF). Labeled protein and free dye were separated on this cation exchange column. Free dye did not bind to the column under these conditions. Bound protein was eluted using a linear NaCl gradient generated by an Äkta Purifier FPLC system (GE Heathcare) up to a final 1 M concentration, buffered by 10 mM MES at pH 5.5. Labeled and unlabeled protein was clearly separated through this process.

2.3 Mass Spectrometry

An electrospray (ESI) time-of-flight (TOF) mass spectrum was acquired for the eluate of the RP-HPLC chromatography described above. A Synapt ESI–Q–TOF (Waters) mass spectrometer employing a Nanomate ESI chip system (Advion) for positive-mode ionization was used. The system was calibrated using a horse-heart myoglobin standard. The recovered protein mass spectrum was deconvoluted using a maximum entropy method using Waters' software, yielding a principal peak with a mass equal to 35,558.05 $\pm$ 3.61 Da, whereas the predicted mass equals 35,556.35 Da. This mass is within error of the calculated predicted mass of the protein with Cy3B covalently attached to the engineered cysteine residue at position 292.

2.4 Protein Storage

Following labeling and bulk characterization, the labeled α-hemolysin monomer was stored in the cation exchange elution buffer with 0.02% (v:v) sodium azide at +4°C.

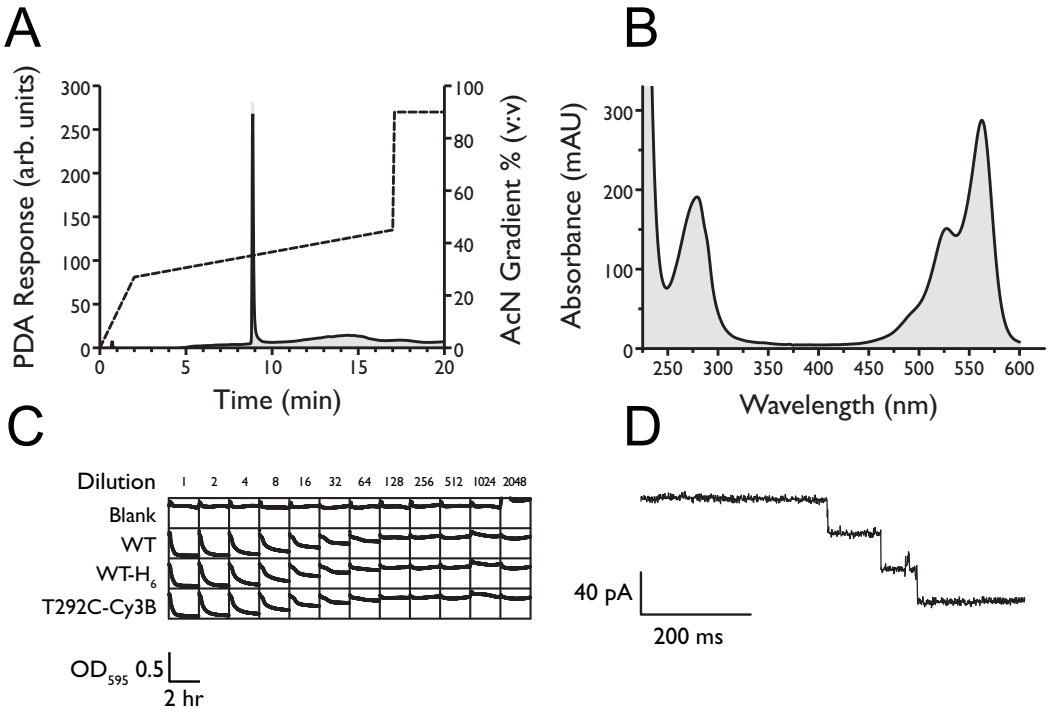

Figure S1: Characterization of Cy3B-labeled α-hemolysin. (A) ARP- HPLC chromatogram showing the separation of the dye-labeled protein from salt by adsorption to and elution from a hydrophobic interaction C18 matrix. (B) Photodiode Array (PDA) spectrum of the peak shown in (A). The Cy3B dye absorbs in the UV and visible spectral regions, however the protein absorbs only in the UV. (C) A hemolytic assay comparing the activities of the wild-type α-hemolysin (WT) from Staphylococcus aureus Wood Strain 46 with hexahistidine-tagged α-hemolysin and Cy3B-labeled α-hemolysin T292C-NRGSGSSSGGSSH6 against rabbit erythrocytes. The protein concentration at the start of the serial dilution is 12.5 nM. Numbers on top of the boxes indicate a serial two-fold dilution going from left to right. The individual box axes correspond to the magnitudes plotted at the bottom left. (D) SCR showing three pore insertion events from labeled α-hemolysin (140 mM NaCl, -50 mV applied potential).

3 Droplet Lipid Bilayer Methods

10 μL of molten 1.5% (w:v) aqueous agarose was deposited on a plasma-cleaned coverslip and dragged across the surface using a second cleaned coverslip to create a thin film. The film was air-dried, leaving a thin coating of dehydrated agarose on the coverslip surface. A micro-channel device made of polymethyl methacrylate (PMMA) was placed on top of the

dried agarose layer[5, 6]. The machined PMMA device consists of a series of wells surrounded by deeper channels which can contact the underlying substrate agarose. These channels serve as a conduit for passing rehydrating molten agarose around the wells. The rehydrating agarose does not significantly enter under the wells, but rather flows around as they are machined to sit 50 μm above the coverslip surface. A protruding lip of rehydrating agarose is generally observed around the rim of the wells occupying no more than 25% of the well-space, not greatly affecting the available optically flat substrate agarose area. The device is designed such that the rehydrated agarose substrate layer is sufficiently thin for the evanescent field to penetrate through to the bilayer. In these experiments, the rehydrating channels were filled with molten 2.5% (w:v) agarose in 10 mM HEPES buffered NaCl (140 mM) at pH 7.4 and allowed to gel.

1,2–diphytanoyl–sn–glycero–3–phosphocholine (DPhPC) (Avanti Polar Lipids Inc., Alabaster, AL) was prepared by dilution from concentrated stocks in chloroform. After solvent evaporation in a N_2 gas stream, lipid was redissolved in hexadecane, yielding a solution concentration of approximately 5 mM. The lipid in oil solution was pipetted into the device wells. After 15 min, an aqueous buffered droplet of approximately 100 nL volume was pipetted into each well, whereafter the droplet sank to the substrate agarose layer at the bottom of the well. A lipid bilayer spontaneously forms at the interface between the agarose substrate and the aqueous droplet.

3.1 Droplet Nano-Injection

Monomeric labeled α-hemolysin was injected into a droplet by nano-injection, visualized with a 10$\times$ magnification objective lens. Borosilicate capillaries were pulled to approximately 10 μm thickness and backfilled with hexadecane prior to attachment to a piezo-driven Nanoliter 2000 injector (World Precision Instruments, Stevenage, U.K.). Protein solution was loaded into the capillary (typically 200 nL) by piston-displacement causing suction. The injector was

manipulated into position through the use of a three-dimensional micromanipulator (Narishige, Japan). A set volume of protein solution (usually 9.2 nL) was then introduced into a droplet by bringing the capillary tip into contact with the droplet and ejecting the solution causing it to fuse with the droplet. The protein-containing droplet was then ready for imaging.

3.2 Single Channel Recording

DHBs were accessed electrically by inserting a 100 m diameter Ag/AgCl electrode into the droplets using a micromanipulator. Using a corresponding Ag/AgCl ground electrode in the hydrated support it was possible to carry out electrical measurements across the bilayer. Currents were recorded with a patch-clamp amplier (Axopatch 200B; Axon Instruments), and digitised at 1 kHz (MiniDigi-1A; Axon Instruments).

4 Microscopy

A fibre-coupled 532 nm circularly polarised, continuous-wave laser beam (Compass 215M, Coherent Inc, Santa Clara, CA) was focussed at the back aperture of an oil immersion objective lens (60$\times$ Plan Apo N.A. 1.4, Nikon Instruments, UK) mounted on an inverted microscope (Ti-Eclipse, Nikon Instruments UK), illuminating the lipid bilayers through TIR at the coverslip surface. The emitted fluorescence was collected through the same objective, transmitted through dichroic (Q565LP) and band-pass (HQ580/60m) filters (Chroma Technology Corp, Rockingham, VT) and imaged using a 128 $\times$ 128 pixel frame-transfer emCCD detector (iXon DU-860, Andor Technology PLC, Belfast, UK). Image sequences were converted to stacked 16-bit Tagged Image File Format (TIFF) bitmaps for analysis.

5 Single-Molecule Fluorescence Experiment Conditions

All experiments were carried out at 24$\pm$1°C . Droplet experiments were performed with 10 mM HEPES buffered NaCl (140 mM) solution at pH 7.4.

6 Single-Molecule Data Analysis

All images were analyzed using ImageJ[7].

6.1 Single-Particle Tracking

Single-particle tracking for spot detection in experiments was performed using the particle tracker plugin developed by the Computational Biophysics Lab at ETH Zurich [8] for ImageJ [7]. Tracks were analysed using code developed in Igor Pro (Wavemetrics).

6.2 Oligomer Intensity Analysis

Droplets were injected with protein and incubated in darkness prior to laser-illumination. Labeled-α-hemolysin could then oligomerize without any fluorophores being photobleached. Upon subsequent laser-illumination, a number of slower diffusing spots were observed, far brighter than the monomers (identified by their single-step photobleaching). The use of a fast acquisition time (2.5 ms integration time) allowed for tracking of the rapidly-diffusing monomers ($D_{lat} \approx 21.5$ μm^2 s^{-1}) on the lipid bilayer [5]. A high laser-intensity was required to resolve the monomers at the fast frame rate. Calibration experiments were performed to gauge the correct detector gain settings to ensure a sufficient dynamic range for relative intensity analyses, with no pixel saturation.

Five separate droplet bilayers were used to generate images for oligomer intensity analysis. A quantile-based normalization algorithm written by Mark Longair at the University of Edinburgh, based upon work by Bolstad *et al.* was used to create a single data-set for

analysis [9]. Originally this algorithm was developed for use when comparing oligonucleotide microarray data. The algorithm finds the maximum and minimum values across all of the images and assigns all pixels into 256 linearly-distributed intensity bins ranging from the global minimum to the global maximum intensity. The images are then reconstructed, with each pixel taking the mean value of the bin it was assigned to. Each fluorescent spot in the normalized images was detected using CLEAN and fitted with a 2D-Gaussian function using an Igor Pro implementation of the algorithm as described previously[5, 10]. The peak intensities are plotted as a histogram with a bin width equal to $3.49 * \sigma * N^{1/3}$, where σ is the standard deviation, and N is the number of fluorescent spots fitted [11].

The resulting spot intensity histogram was fitted with a sum of log-normal and Gaussian probability density functions (PDF) through Levenberg-Marquardt least-squares minimization.

6.3 Photobleaching Steps Analysis

Photobleaching analysis was performed as reported by Das *et al.* [4] using code developed in Igor Pro (Wavemetrics). Fluorescent spot regions of interest (ROIs) measuring 2×2 pixels were detected in images corresponding to all detected spots with intensity above background using CLEAN. Photobleaching tracks were processed by a simplified forward-backward non-linear edge-preserving algorithm described by Chung and Kennedy [12]. Here a single edge-preservation predictor was used. Window size was calculated by fitting the decay of the average of all normalized photobleaching trajectories (each trajectory area normalized to unity) with an exponential function. We then calculated the window size required to observe at least 20 photobleaching steps, in these data the window size was set to 52.5 ms $\times$ 52.5 ms and used for all steps. The algorithm computes a mean and standard deviation in two adjacent running windows. The algorithm then reconstitutes the signal using the mean value of the filter segment with the lowest standard deviation. The reconstituted running average maintains sharp changes

in signal amplitude whilst preserving the underlying properties of the signal [4, 13, 14, 15].

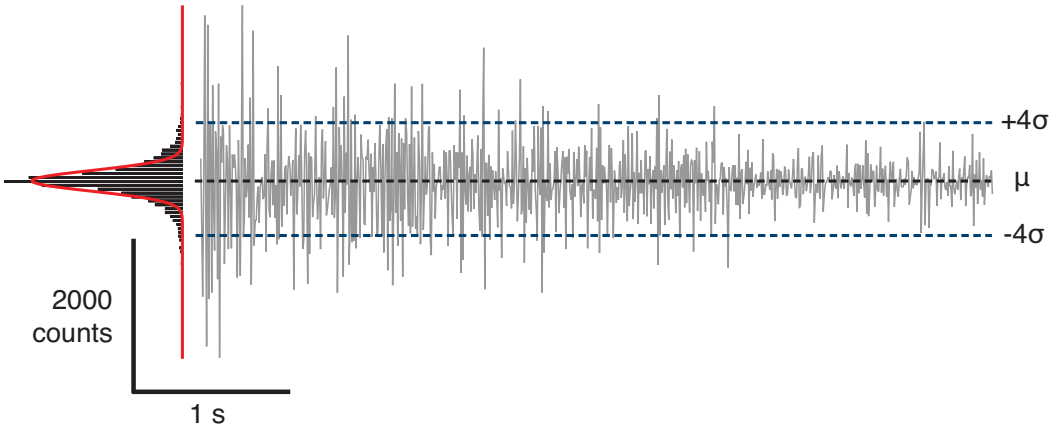

Figure S2: Pairwise difference calculation for the raw unprocessed photobleaching trace shown in Fig 3C in the main text. The difference between point i and i+1 for each point in the photobleaching trace is calculated and plotted versus time. The corresponding pairwise difference is plotted as a histogram and fitted with a Gaussian PDF to give an estimate of the signal noise. Four multiples of the standard deviation is calculated and used in the subsequent step finding algorithm as the step detection threshold.

Step detection due to fluorophore photobleaching was assigned through the definition of a threshold intensity value corresponding to four multiples of the signal noise standard deviation. This was calculated through fitting a pairwise-difference distribution of the original photobleaching trajectory. This distribution is Gaussian (single-molecule intensity noise is assumed to be normally distributed), where the FWHM of the Gaussian is taken as the noise in the signal.

Detection of steps in Chung-Kennedy processed trajectories was performed automatically by defining a step as an intensity jump in the signal of greater than or equal to the established threshold (4 multiples of the calculated noise value). Down-steps minus up-steps (potentially due to single-molecule blinking, or monomers diffusing through the ROI) yields the total number of photobleaching steps.

We then calculated the average detected step size for each individual photobleaching

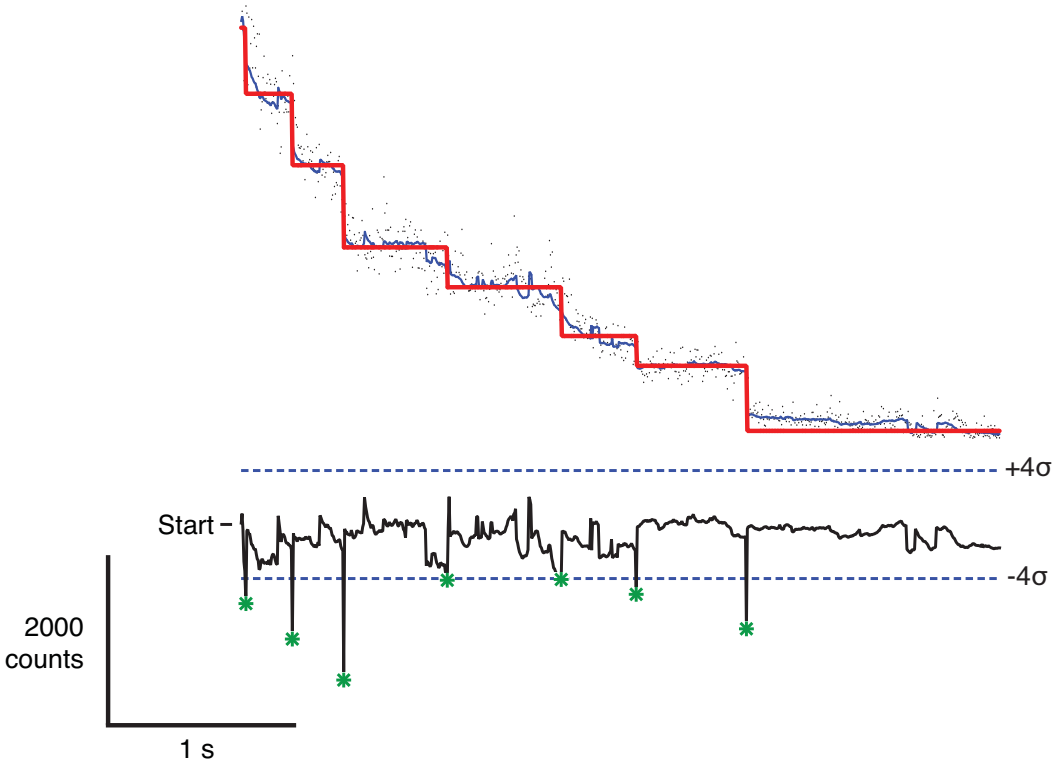

Figure S3: The method for finding steps in a Chung-Kennedy filtered photobleaching trace. An automated detection algorithm runs through the Chung-Kennedy filtered photobleaching trace. Steps are assigned (at data point $i + 1$) if its value is greater than or equal to the threshold from the mean of all data points since the previous detected jump. The mean value of the data points between jumps (bold red line) are plotted over the Chung-Kennedy filtered trace (blue) overlaid atop the raw photobleaching trace data (black spots). These jumps and their thresholds are illustrated below the photobleaching trace, indicated by green stars on a pairwise difference distribution (mean $-i + 1^{th}$ data point) outputted by the automatic algorithm.

trajectory. The initial intensity of each photobleaching trajectory was then divided by its detected average step size value. This gives an estimate of the stoichiometry in the resolved complex (n.b. this will not be a unitary value). These stoichiometries were plotted as a histogram with an optimized bin width given by $3.49 * \sigma * N^{1/3}$, as above, and fitted with a Gaussian PDF to give the subunit stoichiometry.

6.4 Pore Assembly Kinetics Analysis

We used a time-lapse approach to measure the rate of appearance of oligomers in our images. A shuttered laser was triggered every 10 s to yield a 250 ms snapshot of the lipid bilayer. This approach reduces the effect of photobleaching, which under continuous illumination might severely hinder detection of oligomers. ROIs measuring 2×2 pixels in images above background intensity were automatically detected in images using CLEAN, corresponding to all fluorescent spots. Oligomers were assigned when brighter than three multiples of the standard deviation of the monomer intensity (as recovered from a histogram of all PSF intensities). Using this method we were able to count the concentration of monomers and heptamers on the lipid bilayer at each time point.

Concentrations of monomers on the lipid bilayer were evaluated in several ways. Firstly, at concentrations where individual monomers can be resolved the surface concentration was well characterized by counting the monomers. At these concentrations, assembly was rare and heptamers were only detected by leaving the experiment in darkness to avoid photobleaching. Secondly, a known concentration of labeled monomer was injected into a droplet and the high surface monomer concentration was estimated by comparing the background monomer intensity to the intensity of an appearing oligomer, these concentrations allowed us to capture several rapid ($<$5 ms) assembly events. To corroborate this value, the same concentration of monomer was injected into a droplet but with only 2% of the sample labeled, the labeled monomers were

counted as before and the concentration was then linearly-scaled to account for the unlabeled monomers.

6.4.1 2D Collision Kinetics Calculations

Using Eq. 1 from the main text we calculated the rates of collisions of monomers with activated complexes for different encounter radii and surface densities (Figure 4). This shows no significant increase in the time taken for a monomer collision with an activated complex until the encounter radius R exceeds 100 nm for a fixed surface density of monomers (12.34 μm^{-2}). Also, when the surface density drops below $\sim$5 monomers μm^{-2} there is a significant increase in the time taken for monomers to encounter an activated complex with an encounter radius equal to 1 nm.

7 Supplementary Movie

7.1 Rapid Appearance of Oligomers

A movie (5 ms frame integration time) played at 100 frames s^{-1} (half real-time rate). Five 28 $\times$ 28 pixel areas are shown for each separate oligomer appearance, corresponding to an area of lipid bilayer of 114.4 μm^2 at this magnification. Other pre-formed oligomers can be seen in some of the selected areas clearly brighter than the background rapidly diffusing monomers.

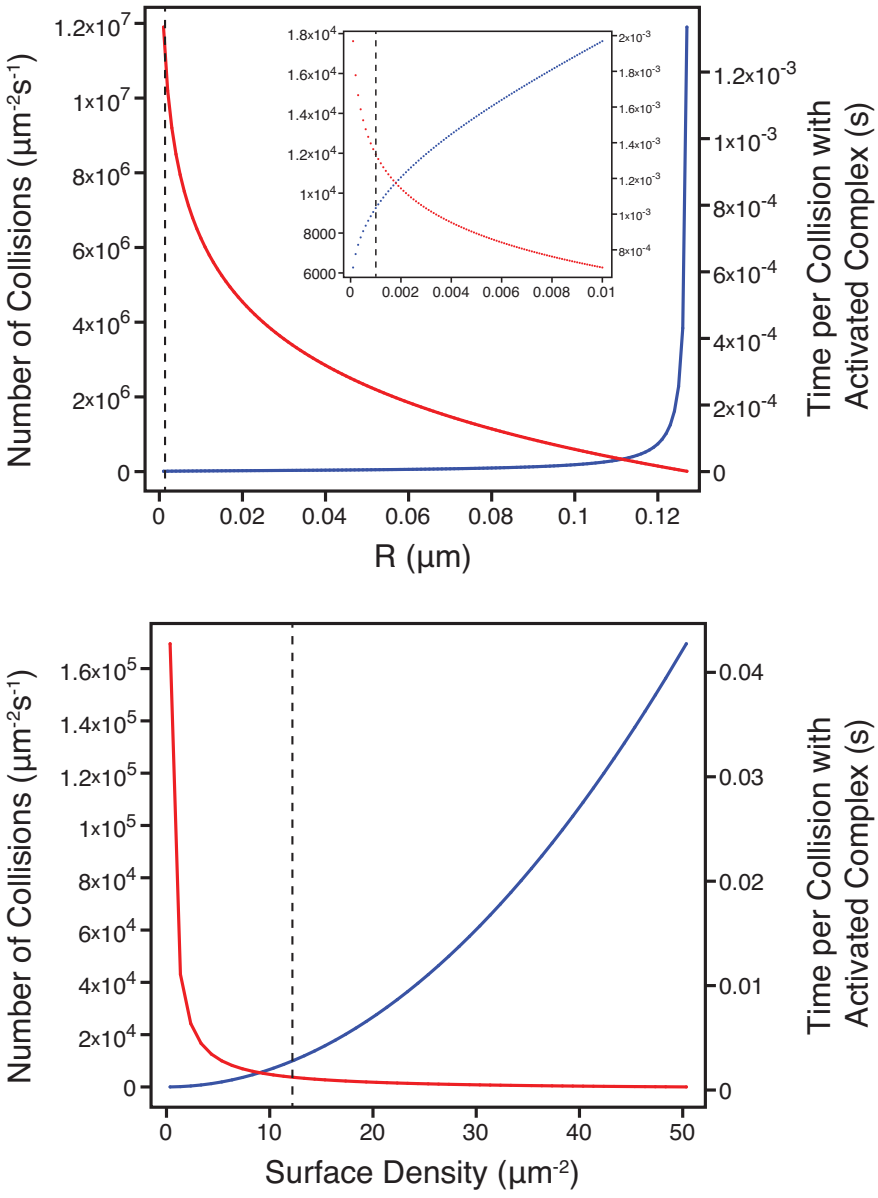

Figure S4: Variation of 2D encounter kinetics parameters. Blue data points indicate the calculated number of monomer collisions, red data points indicate the time required for monomers to encounter an activated complex, both for varying the encounter radius (R) and the surface density of monomers. Dashed vertical lines indicate the parameters used for the calculations described in the main text.

References and Notes

[1] Walker, B. and Bayley, H. Key residues for membrane binding, oligomerization, and pore forming activity of staphylococcal α-hemolysin identified by cysteine scanning mutagenesis and targeted chemical modification. *J. Biol. Chem.* **270**(39), 23065–23071 (1995).

[2] Cheley, S., Malghani, M. S., Song, L., Hobaugh, M., Gouaux, J. E., Yang, J., and Bayley, H. Spontaneous oligomerization of a staphylococcal α-hemolysin conformationally constrained by removal of residues that form the transmembrane β-barrel. *Protein Eng.* **10**(12), 1433–1443 (1997).

[3] Cheley, S., Braha, O., Lu, X., Conlan, S., and Bayley, H. A functional protein pore with a 'retro' transmembrane domain. *Protein Sci.* **8**(6), 1257–1267 (1999).

[4] Das, S. K., Darshi, M., Cheley, S., Wallace, M. I., and Bayley, H. Membrane protein stoichiometry determined from the step-wise photobleaching of dye-labelled subunits. *Chembiochem* **8**(9), 994–999 (2007).

[5] Thompson, J. R., Heron, A. J., Santoso, Y., and Wallace, M. I. Enhanced stability and fluidity in droplet on hydrogel bilayers for measuring membrane protein diffusion. *Nano Lett.* **7**(12), 3875–3878 (2007).

[6] Heron, A. J., Thompson, J. R., Cronin, B., Bayley, H., and Wallace, M. I. Simultaneous measurement of ionic current and fluorescence from single protein pores. *J Am Chem Soc* **131**(5), 1652–3 (2009).

[7] Abramoff, M. D., Magelhaes, P. J., and Ram, S. J. Image processing with ImageJ. *Biophotonics Int.* **11**(7), 36–42 (2004).

[8] Sbalzarini, I. F. and Koumoutsakos, P. Feature point tracking and trajectory analysis for video imaging in cell biology. *J. Struct. Biol.* **151**(2), 182–195 (2005).

[9] Bolstad, B. M., Irizarry, R. A., Astrand, M., and Speed, T. P. A comparison of normalization methods for high density oligonucleotide array data based on variance and bias. *Bioinformatics* **19**(2), 185–193 (2003).

[10] Cronin, B., de Wet, B., and Wallace, M. I. Lucky imaging: improved localization accuracy for single molecule imaging. *Biophys. J.* **96**(7), 2912–7 (2009).

[11] Scott, D. On optimal and data-based histrograms. *Biometrika* **66**, 605–610 (1979).

[12] Chung, S. H. and Kennedy, R. A. Forward-backward non-linear filtering technique for extracting small biological signals from noise. *J. Neurosci. Methods* **40**(1), 71–86 (1991).

[13] Leake, M. C., Wilson, D., Gautel, M., and Simmons, R. M. The elasticity of single titin molecules using a two-bead optical tweezers assay. *Biophys. J.* **87**(2), 1112–1135 (2004).

[14] Leake, M. C., Chandler, J. H., Wadhams, G. H., Bai, F., Berry, R. M., and Armitage, J. P. Stoichiometry and turnover in single, functioning membrane protein complexes. *Nature* **443**(7109), 355–358 (2006).

[15] Haran, G. Noise reduction in single-molecule fluorescence trajectories of folding proteins. *Chem. Phys.* **307**(2-3), 137–145 (2004).